# Experimental and computational studies on the synthesis and structural characterization of 2-(4-chlorophenoxy)-*N*-[4-(4-methylphenyl)-1,3-thiazol-2-yl]acetamide

Hamdi Hamid Sallam [a,b], Yasser Hussien Issa Mohammed [c,d], Fares Hezam Al-Ostoot [c,e], P. Akhileshwari [a], M.A. Sridhar [a,*], Shaukath Ara Khanum [c]

[a] *Department of Studies in Physics, University of Mysore, Manasagangotri, Mysuru 570006, India*
[b] *Department of Physics, Faculty of Education and Science, Taiz University, Turba Branch, Taiz, Yemen*
[c] *Department of Chemistry, Yuvaraja's College, University of Mysore, Mysuru 570006, India*
[d] *Department of Biochemistry, Faculty of Applied Science, University of Hajjah, Hajjah, Yemen*
[e] *Department of Biochemistry, Faculty of Education and Science, Al-Baydha University, Al-Baydha, Yemen*

## ARTICLE INFO

## ABSTRACT

The title compound 2-(4-chlorophenoxy)-*N*-[4-(4-methylphenyl)-1,3-thiazol-2-yl]acetamide **(3)** has been achieved via a sequence of multistep synthesis processes in good yield started by 2-(4-chlorophenoxy)acetic acid **(1)** with 4-(4-methylphenyl)thiazol-2-amine **(2)** in dry dichloromethane followed by the addition of lutidine, and *O*-(benzotriazole-1-yl)-*N,N,N',N'*-tetramethyluroniumtetrafluoroborate as coupling agent in cold condition to accomplish **(3)**. The synthesized compound was elucidated by different spectroscopic techniques (NMR and LC-MS) and finally, the structure was confirmed by X-ray diffraction method. The title compound has crystallized in the orthorhombic crystal system with the space group *Pca2₁*. Density functional theory calculations were carried out to compare the computational values of **(1)** and **(2)** with **(3)**. The frontier molecular orbitals (HOMO-LUMO) and molecular electrostatic potential (MEP) of **(3)** were analyzed. In the crystal structure, intermolecular and intramolecular interactions were observed. Atom N12 represents the chiral center of **(3)** which is connected to four different groups. The stereochemistry of this molecule at N12 is S configuration. Hirshfeld surface studies and 2D fingerprint plots neatly quantify the interactions involved within the structure. Energy frameworks analysis for **(3)** were performed through different intermolecular interaction energies to understand the packing of molecules and to determine the type of the dominant energy.

© 2021 Elsevier B.V. All rights reserved.

## 1. Introduction

Over the years, the drug discovery and design process has undergone significant changes, where the ever-increasing demand for new and effective drugs has resulted in a continuous search for simple and efficient approaches for virtual screening and biological libraries to be developed [1,2]. For these purposes, medicinal chemists have specially appealed to such synthetic methodologies that allow easy access to vast databases of molecules [3]. In medical chemistry, heterocycles represent by far the main classical categories of new drugs that have overwhelming applications both biologically and industrially [4–6]. The heterocyclic nucleus possesses an essential role in drug discovery and acts as a crucial template for the design, synthesis, and development of different therapeutic drugs [7].

Among many of the heterocyclic molecules, thiazoles and their derivatives occupy a major and important position [8]. While thiazole has long been established to be biologically active, there still is significant scientific value in its varying biological characteristics [9]. The class of heterocyclic derivatives known as thiazole is involved in a wide variety of pharmacological activities in many natural and synthetic products, such as anti-fungal [10], anti-viral [11], anti-inflammatory [12], anti-cancer [13], anti-bacterial [14], and anti-convulsant [15] activities which can be well demonstrated by the wide number of drugs comprising this class of compounds. In the market, thiazoles present in several potent pharmacologically active molecules such as sulfathiazol (anti-microbial drug), ritonavir (anti-retroviral drug), abafungin (anti-

---

* Corresponding author at: Department of Studies in Physics, University of Mysore, Manasagangotri, Mysuru 570006, India.

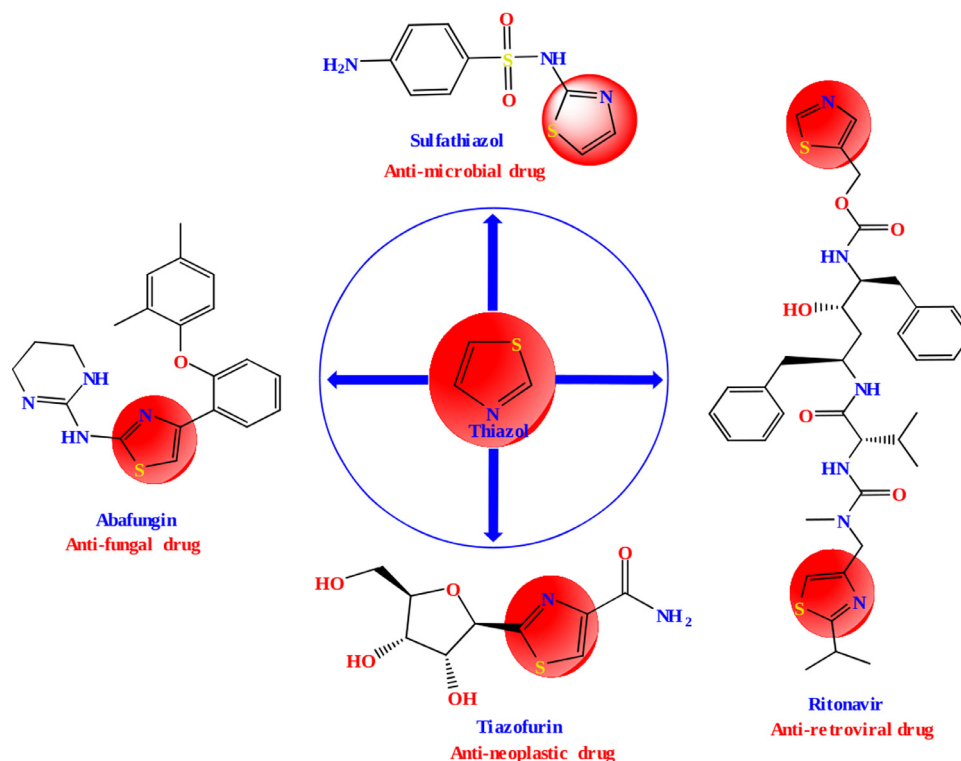*E-mail address:* mas@physics.uni-mysore.ac.in (M.A. Sridhar).

**Fig. 1.** Thiazoles present in several potent pharmacologically active molecules.

fungal drug) and tiazofurin (anti-neoplastic drug), etc [16], Fig. 1. As examples, the anti-convulsant riluzole, anti-parkinsonian talipexole, anti-schistosomal miridazole, anthelmintic tiabendazole and anti-ulcer alizatidine can be cited [17]. In contemporary memory, the applications of thiazoles were found in drug development for the treatment of many diseases for example hypertension, hypnotics, schizophrenia, allergies, and more recently for the treatment of pain and anti-thrombotic activity [16]. The thiazole ring also can be found in other many applications of different fields, such as liquid crystals [18], polymers [19], fluorescent dyes [20], photo-nucleases [21], and finally in insecticides [22]. In view of their broad spectrum of biological properties and as a part of our ongoing work on synthesis and characterization of heterocyclic thiazole derivatives [23,24]. The compound 2-(4-chlorophenoxy)-*N*-[4-(4-methylphenyl)-1,3-thiazol-2-yl]acetamide (**3**) was synthesized and characterized spectroscopically and the molecular structure was confirmed by single crystal X-ray diffraction technique. In this study, we present the experimental and computational results of (**3**) by employing DFT calculations, Hirshfeld surface studies, and 3D energy frameworks analysis.

## 2. Experimental details

### 2.1. Materials and methods

The reagents required for the synthesis of the title compound (ethyl chloroacetate, 4-chlorophenol, 4-(4-methylphenyl) thiazol-2-amine, O-(benzotriazole-1-yl)-*N,N,N',N'*-tetramethyluroniumtetrafluoroborate (TBTU) and lutidine) were procured from Sigma Aldrich Chemical Co. The progress of the reaction was monitored by Thin Layer Chromatography (TLC) performed on aluminium-backed silica plates, and the spots were detected by exposure to UV-lamp at λ= 254 nm. The melting point was measured on a Chemiline, microcontroller based melting point/boiling point-Cl725 apparatus with a digital ther-

mometer. ^{1}H and ^{13}C NMR spectra were recorded on VNMRS-400 Agilent-NMR spectrophotometer. The mass spectra were obtained with a VG70-70H spectrometer. The elemental analysis (C, H, and N) was performed on Elementar Vario EL III elemental analyzer.

### 2.2. 2-(4-chlorophenoxy)-N-[4-(4-methylphenyl)-1,3-thiazol-2-yl]acetamide (3)

A solution of 2-(4-chlorophenoxy)acetic acid (**1**, 2 mmol) was added to 4-(4-methylphenyl)thiazol-2-amine (**2**, 2 mmol) in dry DCM (20 ml), lutidine (3 mmol) at 25-28 °C. The reaction mixture was stirred at the same temperature for half an hour. Then TBTU (2 mmol) was added to the mixture after the temperature was reduced to 0-5 °C [25–27]. Continuously the temperature was maintained below 5 °C for more than half an hour and the reaction mass was stirred overnight. The solvent was evaporated under reduced pressure, quenched by the addition of crushed ice, and the solid obtained was filtered and dried. The crude product upon recrystallization with ethanol and acetonitrile afforded (**3**) as colourless rectangular block shape crystals.

Yield 85%; M.P 174-177 °C; ^{1}H NMR (400 MHz, DMSO) $\delta$ (ppm): 2.19 (*s*, 3H, CH$_3$), 4.80 (*s*, 2H, OCH$_2$), 6.81-7.89 (*m*, 9H, Ar-H), 12.45 ((bs, 1H, NH); ^{13}C NMR (100 MHz, DMSO) $\delta$ (ppm): 20.48, 66.65, 109.51, 114.85, 127.84, 129.19, 130.26, 130.42, 132.74, 165.04, 133.51, 148.13, 156.11, 157.95, 167.69; LC-MS *m/z* 359 [M+], 361 [M+2]. Anal. Calcd. For C$_{18}$H$_{15}$ClN$_2$O$_2$S (359): C, 60.25; H, 4.21; N, 7.81. Found: C, 60.20; H, 4.18; N, 7.80%.

### 2.3. XRD data collection, structure solution and refinement

A colourless rectangular block of (**3**) with approximate dimensions 0.10 × 0.15 × 0.20 mm$^3$ was chosen for X-ray data collection. The data were collected on a Bruker CCD diffractometer equipped with MoK$_\alpha$ radiation with wavelength 0.71073 Å [28] at 296 K. Data were corrected for absorption effects using the

**Table 1**
The crystal data and structure refinement details.

| Parameter | Value |
|---|---|
| CCDC No. | 1868543 |
| Empirical formula | $C_{18} H_{15} Cl N_2 O_2 S$ |
| Formula weight | 358.84 |
| Temperature | 296(2) K |
| Wavelength | 0.71073 Å |
| $\theta$ range | 1.03º to 25.55º |
| Crystal system, Space group | Orthorhombic, $Pca2_1$ |
| Cell parameters | $a = 14.205(3)$ Å |
| | $b = 19.812(4)$ Å |
| | $c = 5.742(1)$ Å |
| Volume | 1616.0(5) Å$^3$ |
| Z | 4 |
| Density(calculated) | 1.475 Mg m$^{-3}$ |
| Absorption coefficient | 0.379 mm$^{-1}$ |
| $F_{000}$ | 744 |
| Crystal size | 0.10 mm × 0.15 mm × 0.20 mm |
| Index ranges | $-17 \leq h \leq 16$ |
| | $-23 \leq k \leq 17$ |
| | $-6 \leq l \leq 6$ |
| Reflections collected | 8463 |
| Independent reflections | 2984 [R $_{int}$ = 0.0458] |
| Absorption correction | Multi-scan |
| Refinement method | Full matrix least-squares on $F^2$ |
| Data / restraints / parameters | 2984 / 1 / 218 |
| Goodness-of-fit on $F^2$ | 1.013 |
| Final [$I > 2\sigma(I)$] | R = 0.0526, wR$_2$ = 0.1104 |
| $R$ indices (all data) | R1 = 0.1325, wR$_2$ = 0.1738 |
| Largest diff. peak and hole | 0.295 and $-0.332$ e Å$^{-3}$ |

multi-scan method. The structure has been solved and refined by adopting *SHELXS-97* and *SHELXL-97* [29] programs respectively. The non-hydrogen atoms were refined anisotropically. Hydrogen atoms were added at calculated positions and allowed to ride on their parent atoms. The geometrical calculations were carried out using *PLATON* software [30]. The molecular packing diagrams were generated using *Mercury* [31]. The crystal data and refinement details of **(3)** are presented in Table 1. This compound has CCDC No. **1868543** at the Cambridge Crystallographic Data Centre where full crystallographic data (CIF) has been deposited.

### 2.4. Computational studies

The density functional theory (DFT) computations for the compounds **(1), (2)** and **(3)** were performed using *Gaussian 09* software [32]. They were carried out with Becke three parameter for the exchange with correlation functional of Lee-Yang-Parr (B3LYP) for $6-31 + G$(d,p) basis sets. The frontier molecular orbitals (HOMO-LUMO) and molecular electrostatic potential (MEP) map were generated for the geometrically optimized structure of **(3)** with the same basis set levels. The Hirshfeld surface analysis and 3D energy frameworks calculations for **(3)** have been studied by employing *CrystalExplorer-17* program [33].

## 3. Results and discussions

### 3.1. The synthesis and characterization of compound (3)

The schematic diagram of the synthesized compound is shown in Fig. 2. Initially, 2-(4-chlorophenoxy)acetic acid **(1)**, was treated with 4-(4-methylphenyl)thiazol-2-amine **(2)**, in dry DCM followed by the addition of lutidine, and TBTU in cold condition to achieve 2-(4-chlorophenoxy)-*N*-[4-(4-methylphenyl)-1,3-thiazol-2-yl]acetamide **(3)**. Finally, the crude product upon re-crystallization with ethanol and acetonitrile afforded the title **(3)** as colourless rectangular block shape crystals.

Furthermore, the synthesized compound has been proved by ^{1}H NMR, ^{13}C NMR, and mass spectra characterization (refer Figs S1–S3 of supplementary file). The ^{1}HNMR spectrum of **(3)** showed the disappearance of the protons of the carboxyl group as well as the amino group of the compounds **(1)** and **(2)**, respectively, and also the appearance of new proton for the N-H group at $\delta$ 12.45 ppm. Besides, the compound **(3)** was also supported by inspecting the ^{13}C NMR and mass spectrum with significant stable [M+] and [M+2] peaks at *m/z* 359 and 361 which clearly affirmed the formation of **(3)**.

### 3.2. Conformational analysis of compound (3)

Single crystal X-ray diffraction technique revealed that the compound **(3)** crystallizes in the orthorhombic crystal system with the space group $Pca2_1$ and the unit cell constants are: $a = 14.205(3)$ Å, $b = 19.812(4)$ Å, $c = 5.742(1)$ Å, and Z = 4. The *ORTEP* of the compound is shown in Fig. 3.

The molecule consists of three rings chloro-phenoxy ring [C2-C3-C4-C5-C6-C7], thiazole ring [C13-N14-C15-C16-S17] and methyl-phenoxy ring [C18-C19-C20-C21-C22-C23]. All the rings in the structure are in planar conformation. The maximum deviation from the plane for the thiazole ring is 0.007(6) Å for C16, while the maximum deviation from the plane for the chloro-phenoxy ring and methyl-phenoxy ring are -0.016(6) Å and 0.004(7) Å for C5 and C22 respectively. The chlorine atom is planar with the (C2/C7) ring as indicated by 180.0(5)º torsion angle for the atoms Cl1-C2-C3-C4. The chloro-phenoxy ring is coplanar with the mean plane of the thiazole ring as the torsion angles between the mean plane of (C2/C7) and (C13/S17) rings are 163.7(5)º and 167.0(5)º, for the atoms C5-O8-C9-C10 and C9-C10-N12-C13 respectively. The chloro-phenoxy ring has nearly typical hexagonal as the bond angle around each atom in the ring is nearly equal to 120º (C3-C2-C7 = 120.0(7)º, C2-C7-C6 = 119.1(7)º, C5-C6-C7 = 120.3(7)º, C2-C3-C4 = 121.3(6)º, C4-C5-C6 = 120.3(7)º). The methyl group at the end of the molecular structure is planer with the methyl-phenoxy ring, where the torsion angle for the atoms C19-C20-C21-C24 is $-177.9(6)$º. This ring is almost planer with thiazole ring as indicated by 174.6(6)° torsion angle for C19-C18-C15-C16 atoms (+anti-periplanar conformation). The methyl group shows distortion in (C18/C23) ring yielding an angle smaller than 120º at the position of substitution i.e., C20-C21-C22 = 116.9(7)º. Selected bond lengths, bond angles and torsion angles of **(3)** are listed in Table 2.

In the structure, atom N12 is a chiral center which is connected to four different groups [34] (a hydrogen atom, C10 or carbonyl group, C13 in thiazole ring, and a lone pair). Since there is only one chiral center in this molecule, there are two probabilities, either R or S configuration (stereocenter). R configuration means a clockwise direction, while S configuration means an anti-clockwise direction. Assigning priority to each of those four groups is based on atomic mass with the extended chain. Here, a lone pair is ignored and the remaining groups are to be considered. C13 in thiazole ring has priority 1 as the atomic number of sulphur is larger than oxygen, carbonyl group has priority 2 and the hydrogen atom is of priority 3. If one follows the numbers of priority 1, 2 and 3, it is found that the direction is anti-clockwise. So the stereochemistry of the molecule at N12 is S configuration.

The structure exhibits intermolecular hydrogen bond interaction of the type C9-H9A...O11 with a bond length of 3.398(8) Å that links the molecules into chains along *c* axis as shown in Fig. 4. Intramolecular hydrogen bond of the type C–H••N exists between C19 and N14 which plays a role in the stabilization of the molecule. The hydrogen bond interactions with the geometry details are listed in Table 3. Additionally, there are three C-H...Cg interactions as listed in Table 4.
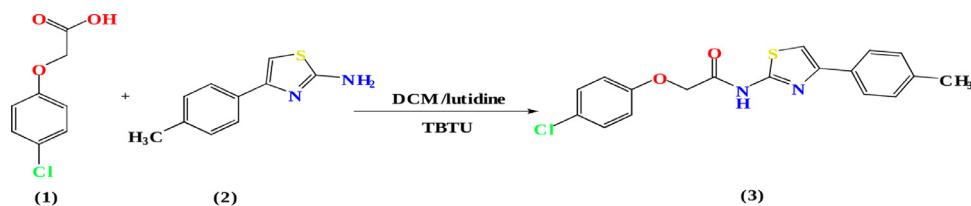
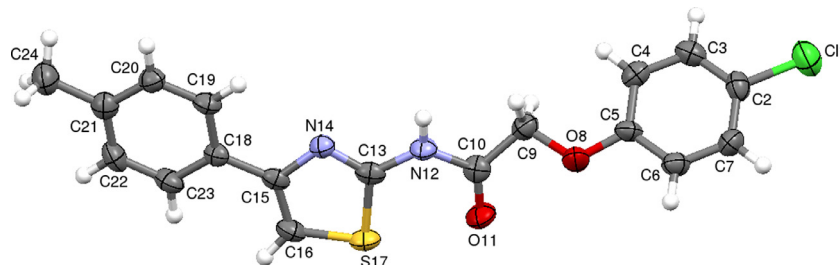**Fig. 2.** Reaction pathway for the synthesis of the title compound **(3)**.



**Fig. 3.** *ORTEP* of **(3)** with thermal ellipsoids drawn at 50% probability.

**Table 2**
Selected bond lengths, bond angles and torsion angles of **(3)**.

| Atoms | Bond lengths (Å) | | Atoms | Bond angles (°) | | Atoms | Torsion angles (°) | |
|---|---|---|---|---|---|---|---|---|
| | XRD | DFT | | XRD | DFT | | XRD | DFT |
| Cl1-C2 | 1.730(8) | 1.7298 | C3-C2-C7 | 120.0(7) | 119.97 | Cl1-C2-C3-C4 | 180.0(5) | 179.97 |
| C2-C7 | 1.39(1) | 1.3932 | C2-C7-C6 | 119.1(7) | 119.13 | C5-O8-C9-C10 | 163.7(5) | 163.65 |
| O8-C9 | 1.414(7) | 1.4141 | O8-C5-C6 | 114.6(6) | 114.64 | O8-C9-C10-O11 | −35.6(9) | -35.64 |
| N14-C13 | 1.29(1) | 1.2875 | C13-S17-C16 | 87.5(4) | 87.55 | C16-S17-C13-N14 | −0.5(5) | -0.54 |
| S17-C16 | 1.715(6) | 1.7150 | C16-C15-C18 | 127.4(6) | 127.37 | C16-C15-C18-C23 | −7(1) | -6.73 |
| C21-C24 | 1.51(1) | 1.5078 | C20-C21-C22 | 116.9(7) | 116.92 | C19-C20-C21-C24 | −177.9(6) | 177.69 |

**Table 3**
Hydrogen bonds geometry of **(3)**.

| D-H … A | D-H (Å) | H… A (Å) | D… A (Å) | D-H … A (°) | Symmetry codes |
|---|---|---|---|---|---|
| C9-H9A...O11 | 0.97 | 2.54 | 3.398(8) | 148 | *1/2-x,y,1/2+z* |
| C19-H19..N14 | 0.93 | 2.53 | 2.858(8) | 101 | Intramolecular |

**Table 4**
C-H...Cg interactions.

| C-H...Cg | H-Cg (Å) | C...Cg (Å) | γ (°) | C-H..Cg (°) | Symmetry codes |
|---|---|---|---|---|---|
| C3-H3...Cg(2) | 2.76 | 3.472(6) | 9.79 | 134 | *1/2-X,Y,1/2+Z* |
| C9-H9B...Cg(3) | 2.78 | 3.645(7) | 11.31 | 150 | *1-X,-Y,1/2+Z* |
| C24-H24C...Cg(2) | 2.80 | 3.697(8) | 7.95 | 156 | *1-X,-Y,-1/2+Z* |

**Cg(2)** is the centroid of the ring (C2/C7) and **Cg(3)** is the centroid of the ring (C18/C23).

### 3.3. DFT computations

The density functional theory (DFT) is a technique widely used in material science to explain the various electronic transitions and chemical properties of the compound. It is an important tool to investigate the properties like geometry optimization, frontier molecular orbital analysis, and molecular electrostatic potential. The optimized structure of compound **(3)** is shown in Fig. 5. DFT calculations depend on the electron density distribution function of the studied compound. The calculated bond lengths, bond angles, and torsion angles of **(3)** are compared with the reactants compounds **(1)** and **(2)**. The theoretical values of the compounds are almost identical as listed in Tables S1–S3 in the supplementary file.

### 3.3.1. Frontier molecular orbitals and global reactivity descriptors

The chemical reactivity and kinetic stability of any compound depends on the frontier molecular orbitals (HOMO-LUMO) and the energy gap between them. The frontier molecular orbitals and the

energy gap for the title compound are shown in Fig. 6. The energy gap for the compound is 4.569 eV, which describes the hardness of the compound and the difficult transfer of electrons from HOMO to LUMO [7].

The global chemical reactivity descriptors enable us to know the chemical properties of the compound. Ionization potential (I) is a measure of electron donating power of a molecule which is calculated by $I = -E_H$. The electron affinity (A) characterizes the ability of a molecule to accept electrons and it is given as $A = -E_L$. The difference between ($E_L$) and ($E_H$) is the energy gap ($\Delta E$), which determines the hardness, softness and chemical reactivity of the molecule. The chemical hardness ($\eta$) is one-half of the energy gap i.e., $\eta = \Delta E / 2$, while global softness ($\sigma$) of the molecule is calculated by the formula $\sigma = 1 / 2\eta$. Chemical potential ($\mu$) of the molecule is expressed as $\mu = E_H + E_L / 2$. Electronegativity ($\chi$) is the tendency of an atom in a molecule to attract shared electrons and it is given by $\chi = - \mu$. Eletrophilicity ($\omega$) specifies the
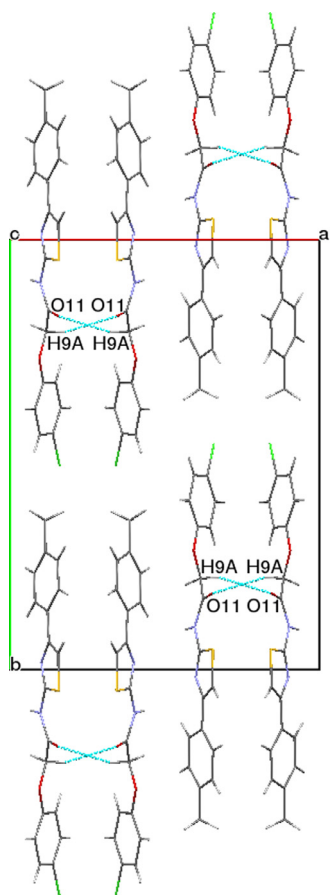
**Fig. 4.** The packing of the molecules along *c* axis involving C-H...O hydrogen bonds.
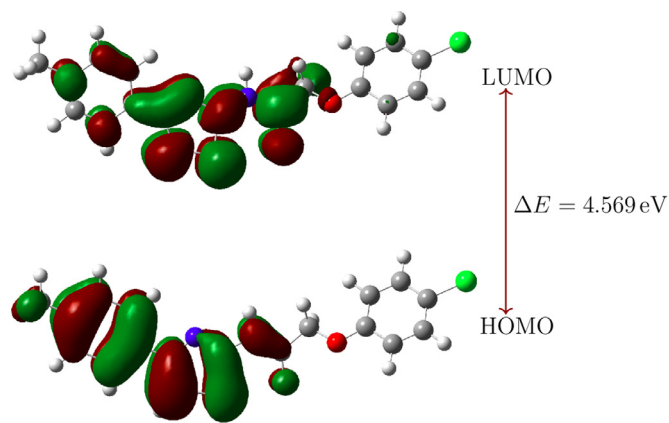


**Fig. 6.** HOMO-LUMO and energy gap of **(3)**.

**Table 5**

Calculated energy values and quantum molecular descriptors of **(3)**.

| Parameters | Symbol and formula | Values |
|---|---|---|
| HOMO energy | $E_H$ (eV) | -5.695 |
| LUMO energy | $E_L$ (eV) | -1.126 |
| Energy gap | $\Delta E = E_L - E_H$ (eV) | 4.569 |
| Ionization potential | $I = - E_H$ (eV) | 5.695 |
| Electron affinity | $A = - E_L$ (eV) | 1.126 |
| Chemical hardness | $\eta = \Delta E / 2$ (eV) | 2.285 |
| Global softness | $\sigma = 1/ 2\eta$ (eV$^{-1}$) | 0.219 |
| Chemical potential | $\mu = E_H + E_L / 2$ (eV) | -3.411 |
| Eletronegativity | $\chi = - \mu$ (eV) | 3.411 |
| Eletrophilicity | $\omega = \mu^2 / 2\eta$ (eV) | 2.546 |

electrophilic power of a molecule and is calculated by $\omega = \mu^2 / 2\eta$ [32]. The energy gap and the other global reactivity descriptors for the studied compound are listed in Table 5.

### 3.3.2. Molecular electrostatic potential (MEP)

The molecular electrostatic potential (MEP) is a 3D map representing the charge distribution of the molecule. This map shows the colour scheme that is scaled from the deepest red maximum electron concentration (-6.828e−2 a.u.) to the deepest blue maximum electron deficient (+6.828e−2 a.u.) for **(3)**. The different colors on electrostatic potential map determine the nucleophilic or electrophilic reactive sites [24]. The MEP of the studied compound (Fig. 7) illustrates the maximum electron concentration around O11 atom, nucleophilic site, and the maximum electron de-

ficient around H9A atom, electrophilic site. This is due to the C9-H9A...O11 hydrogen bond in **(3)** (see Subsection 3.2). The obtained result indicates that the reactive sites of the molecule can interact with the neighboring molecules.

### 3.4. Hirshfeld surface studies

The Hirshfeld surface is a powerful graphical visualization tool for realising the intermolecular interactions of the studied compound. Hirshfeld surface volume and surface area of **(3)** are 395.92 Å$^3$ and 379.37 Å$^2$ respectively. The close intermolecular contacts can be shown on the Hirshfeld surface map by calculating normalized contact distance $d_{norm}$ (Fig. 8). This mapping shows red, blue, and white color regions. The normalized contact distance $d_{norm}$ is defined as

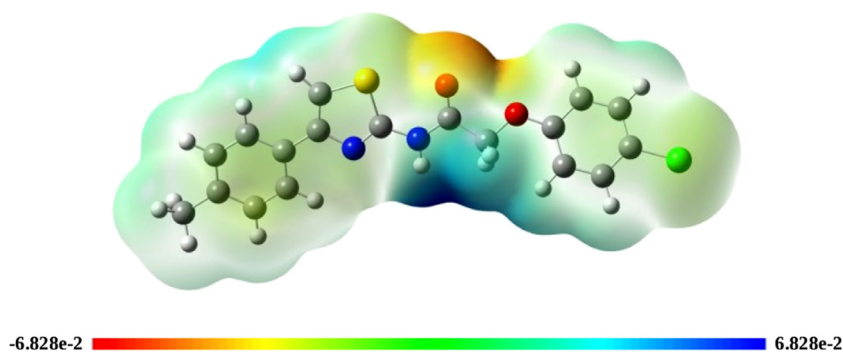$$d_{norm} = \frac{d_i - r_i^{vdW}}{r_i^{vdW}} + \frac{d_e - r_e^{vdW}}{r_e^{vdW}},$$



**Fig. 5.** The optimized structure of **(3)** at DFT/B3LYP/6-31+G(d,p) level.

**Fig. 7.** Molecular electrostatic potential map of (**3**).
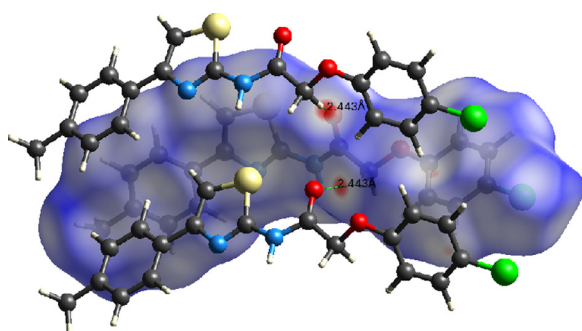


**Fig. 8.** Hirshfeld surface of (**3**) mapped over $d_{norm}$.

**Table 6**
Contribution of different intermolecular interactions in percentages (%).

| Interaction | Contribution (%) |
|---|---|
| C-H | 30.9 |
| H-H | 27.6 |
| O-H | 13.2 |
| Cl-H | 11.7 |
| S-H | 4.5 |
| N-H | 3.9 |

where, $d_i$ and $d_e$ are the distances from each point on the surface to the nearest nuclei internal and external to the surface, respectively. $r_i^{vdW}$ and $r_e^{vdW}$ are the van der Waals radii of the atoms internal and external to the surface, respectively. The value of $d_{norm}$ can be negative (red regions) or positive (blue regions) depending on contacts that are shorter or longer than the van der Waals radii respectively; whereas the white colored regions represent the contacts which are equal to the van der Waals radii or $d_{norm}$ = zero [35]. The two bright red regions on the surface are due to C9-H9A...O11 intermolecular hydrogen bonds. It is clear that, the Hirshfeld surface analysis of (**3**) confirms the existance of intermolecular hydrogen bond (C9-H9A...O11) which is responsible for linking

the molecules in the crystal as it was revealed from the crystallographic analysis (see Subsection 3.2).

### 3.4.1. 2D fingerprint plots

Two dimensional fingerprint plots were generated to reveal the percentage of the intermolecular contributions of intermolecular interactions of each type of contact to the total Hirshfeld surface area [36]. The Fingerprint plots were mapped by using the translated 1–3 Å, and filtering by element. The decomposed fingerprint plots are shown in Fig. 9a–f. The major contribution is from C-H contacts, which contribute the most (30.9%) to the total Hirshfeld surface area. The remaining contributions are from H-H, O-H, Cl-H, S-H, N-H contacts. The contributions from different interactions to the total Hirshfeld surface area are listed in Table 6. The strong intermolecular interactions appear as distinct spikes in the fingerprint plots. O-H interactions appear as two characteristic spikes (Fig. 9c) which have a significant contribution to the crystal pack-

**Table 7**
Different interaction energies of the molecular pairs in kJ/mol.

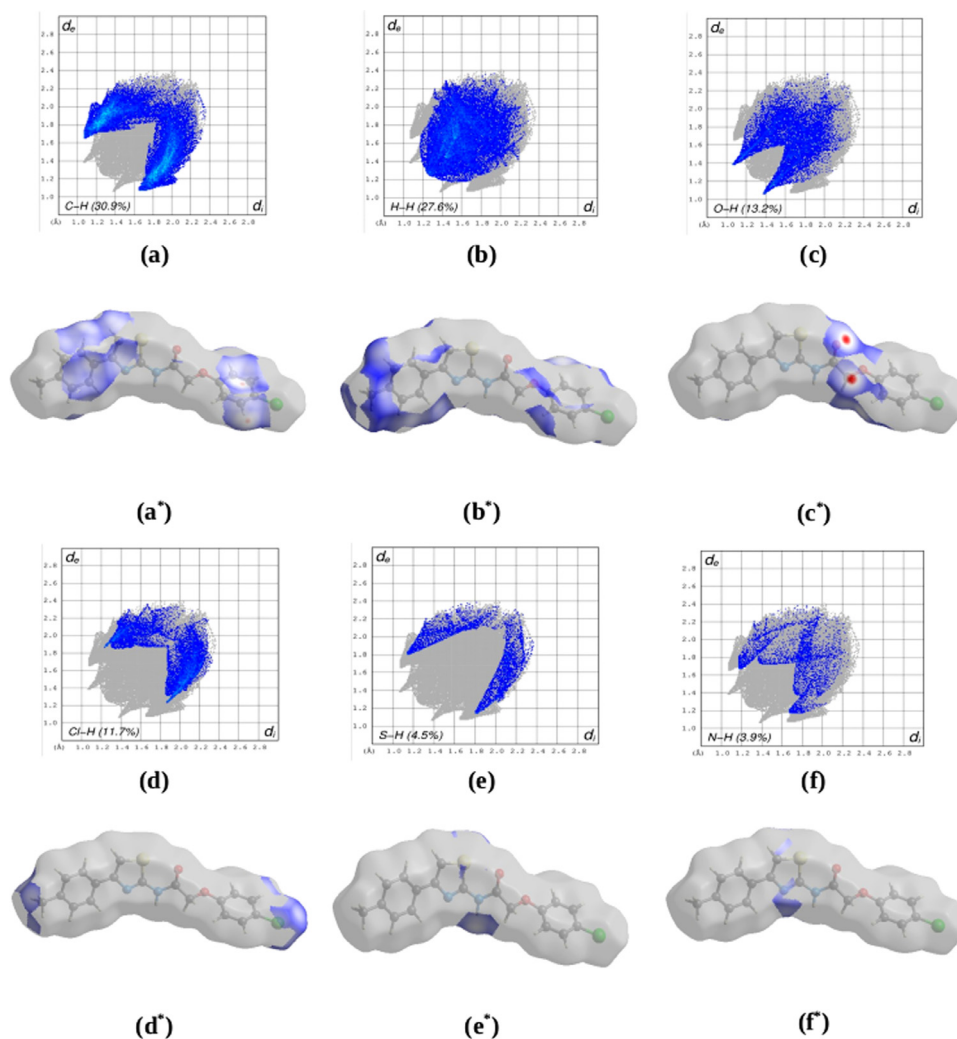|  | N | Symmetry operation | R (Å) | Electron Density | E_ele | E_pol | E_dis | E_rep | E_tot |
|---|---|---|---|---|---|---|---|---|---|
| 🟥 | 2 | x, y, z | 5.74 | B3LYP/6-31G(d, p) | -25.2 | -5.8 | -44.8 | 31.6 | -50.4 |
| 🟧 | 2 | -x+1/2, y, z+1/2 | 4.54 | B3LYP/6-31G(d, p) | -13.0 | -5.2 | -68.9 | 47.1 | -48.4 |
| 🟩 | 2 | -x, -y, z+1/2 | 6.51 | B3LYP/6-31G(d, p) | -14.1 | -6.0 | -67.0 | 40.2 | -52.9 |
| 🟩 | 2 | x, y, z | 20.63 | B3LYP/6-31G(d, p) | -1.1 | -0.1 | -4.8 | 3.2 | -3.4 |
| 🟦 | 2 | -x+1/2, y, z+1/2 | 20.33 | B3LYP/6-31G(d, p) | -1.0 | -0.1 | -3.1 | 2.3 | -2.5 |
| 🟦 | 2 | x, y, z | 19.81 | B3LYP/6-31G(d, p) | -1.0 | -0.2 | -5.8 | 3.3 | -4.2 |
| 🟪 | 2 | -x, -y, z+1/2 | 15.88 | B3LYP/6-31G(d, p) | -1.2 | -0.4 | -9.0 | 5.0 | -6.3 |

**Fig. 9.** (a), (b), (c), (d), (e), (f) are the 2D fingerprint plots showing each decomposed contact with the percentage contribution and (a*), (b*), (c*), (d*), (e*), (f*) represent the associated $d_{norm}$ Hirshfeld surfaces. The full fingerprint plot appears as a gray shadow below each decomposed plot.
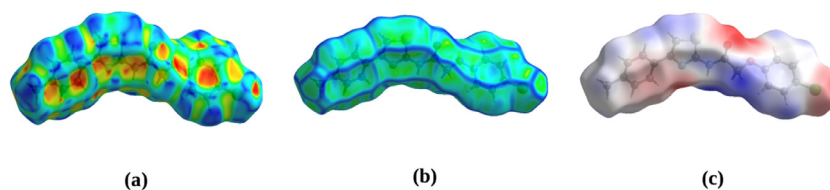


**Fig. 10.** Hirshfeld surface with (a) shape index, (b) curvedness and (c) electrostatic potential map.

ing where the distance $d_i + d_e \approx 2.4$ Å respectively (i.e., shorter than van der Waals radii).

### 3.4.2. Shape index, curvedness, and electrostatic potential map

The shape index throws light on the stacking arrangement of molecules. The shape index map (Fig. 10a) is used to identify the complementary hollows (red) and bumps (blue) where two molecular Hirshfeld surfaces touch each other. These red and blue colored triangular shaped patterns are the representation of a particular stacking arrangement of molecules [37].

Curvedness map conveys the magnitude of the surface curvature [38]. It is characterized by relatively large green colored regions, separated by dark blue 'edges' as shown in Fig. 10b. The surface is mapping from -4.0 to +0.4 and has been found to be useful with molecular Hirshfeld surfaces. Since there is no flat surface

seen on the curvedness plot, there is no planar stacking between the molecules.

The blue and red colored regions on the electrostatic map represent the electropositive and electronegative regions respectively for the studies compound [37]. On the electrostatic map, the bright red colored region is the electronegative region, which localized on O11 atom and blue colored region is the electropositive region, which exists around C9-H9A atoms (Fig. 10c).

### 3.5. Energy frameworks analysis on interaction energies

The total interaction energy of (3) was calculated by generating a cluster of molecules within a radius of 3.8 Å around the selected molecule. The scale factors for standard energies used for the construction of energy models were taken from Mackenzie *et al.* $k\_ele = 1.057$, $k\_pol = 0.740$, $k\_disp = 0.871$, $k\_rep = 0.618$
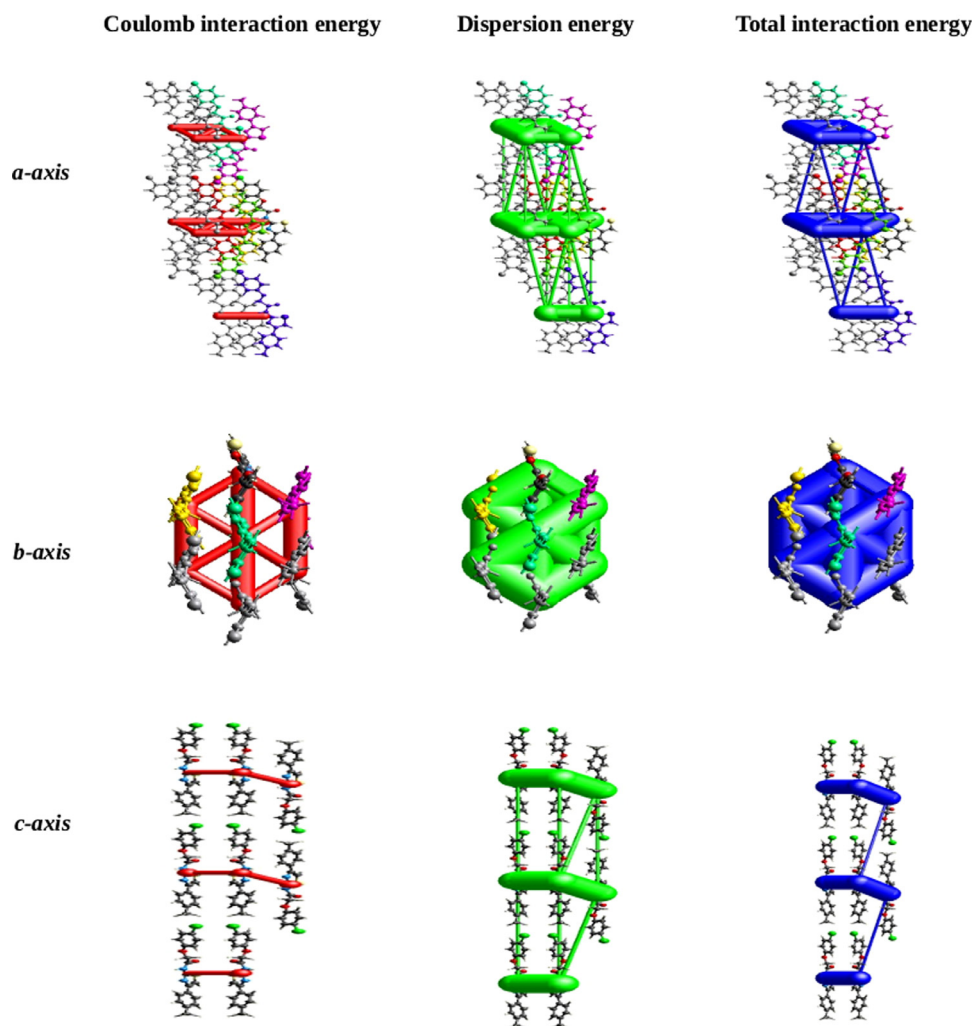
**Fig. 11.** The graphical representation of electrostatic interactions Coulomb interaction energy, dispersion energy, and total interaction energy of **(3)** along different axes.

[39]. Table 7 lists the calculated interaction energies in kJ/mol and the symmetry operations for seven molecules. The red colored molecule with symmetry operation (*x,y,z*) located at 5.74 Å from the centroid of the selected molecule showing the highest total interaction energy (-50.4 kJ/mol) whereas the turquoise colored molecule with symmetry operation (*-x+1/2, y, z+1/2*) located at 20.33 Å from the centroid of the selected molecule exhibits the lowest total interaction energy (-2.5 kJ/mol). The total interaction energy of the compound is -168.1 kJ/mol. The calculated interaction energies for electrostatic, polarization, dispersion, and repulsion are -56.6 kJ/mol, -17.8 kJ/mol, -203.4 kJ/mol, and 132.7 kJ/mol respectively. The dispersion interaction energy dominates over the electrostatic energy frameworks. The visualization of 3D energy frameworks of **(3)** was generated for the above energy terms and represented in terms of different colored cylinders along with different directions (Fig. 11). There is an absence of cylinders in some directions due to the exclusion of a few interactions under certain threshold energy. These weaker interactions ignored only to make the figures less crowded [40].

## 4. Conclusions

In conclusion, phenyl thiazole acetamide **(3)** was achieved in excellent yield and its structure was analyzed by spectroscopic and XRD techniques. This compound ($C_{18}H_{15}ClN_2O_2S$) crystallizes in the orthorhombic crystal system with the *Pca2$_1$* space group. Crystal structure of the compound stabilized by C-H...O intermolecular and C-H...N intramolecular hydrogen bonds. The strucure has one chiral center (atom N12) and the stereochemistry of **(3)** at this atom is S configuration. DFT calculations show very good agreements between the computational values of the reactants **(1)** and **(2)** with compound **(3)**. The high energy gap (4.569 eV) between the frontier molecular orbitals implies the stability of **(3)**. The charge distribution on the MEP map shows nucleophilic and electrophilic sites in the molecule. Hirshfeld surface studies confirm the existance of intermolecular hydrogen bond (C9-H9A...O11) and 2D fingerprint plots show that the major contribution is from C-H contacts with 30.9%. The crystal packing of **(3)** was performed using the concept of 3D energy frameworks analysis and found that dispersion energy is the dominant value (-203.4 kJ/mol) among all interaction energies.

## Declaration of Competing Interest

The authors declare that they have no known competing financial interests or personal relationships that could have appeared to influence the work reported in this paper.

## CRediT authorship contribution statement

**Hamdi Hamid Sallam:** Formal analysis, Data curation, Calculations, Investigation, Software, Visualization, Conceptualization, Methodology, Writing original draft. **Yasser Hussien Issa Mohammed** and **Fares Hezam Al-Ostoot:** Formal analysis, Investigation, Writing original draft. **Akhileshwari P.:** Formal analysis. **Sridhar M.A.** And **Shaukath Ara Khanum:** Supervision, Approving original draft.

## Acknowledgments

## Supplementary materials

Supplementary material associated with this article can be found, in the online version, at doi:10.1016/j.molstruc.2021.131588.

## References

[1] C. Sahlgren, A. Meinander, H. Zhang, F. Cheng, M. Preis, C. Xu, T.A. Salminen, D. Toivola, D. Abankwa, A. Rosling, D.Ş. Karaman, Tailored approaches in drug development and diagnostics: from molecular design to biological model systems, Adv. Healthc. Mater. 6 (2017) 1–34.

[2] F.H. Al-Ostoot, S. Salah, S.A. Khanum, Recent investigations into synthesis and pharmacological activities of phenoxy acetamide and its derivatives (chalcone, indole and quinoline) as possible therapeutic candidates, J. Iran. Chem. Soc. 1 (2021) 1–37.

[3] C.J. Gerry, S.L. Schreiber, Chemical probes and drug leads from advances in synthetic planning and methodology, Nat. Rev. Drug Discov. 17 (2018) 333–352.

[4] M.N.K. Zabiulla, A.B. Begum, M.K. Sunil, S.A. Khanum, Synthesis, docking and biological evaluation of thiadiazole and oxadiazole derivatives as antimicrobial and antioxidant agents, Results Chem. 2 (2020) 1–14.

[5] S.A. Al-horaibi, A.A. Alrabie, M.T. Alghamdi, F.H. Al-Ostoot, E.M. Garoon, A.S. Rajbhoj, Novel hemicyanine sensitizers based on benzothiazole-indole for dye-sensitized solar cells: synthesis, optoelectrical characterization and efficiency of solar cell, J. Mol. Struct. 1224 (2021) 1–18.

[6] N. Abad, H.H. Sallam, F.H. Al-Ostoot, H.A. Khamees, S.A. Al-horaibi, S.A. Khanum, M. Madegowda, M. El Hafi, J.T. Mague, E.M. Essassi, Y. Ramli, Synthesis, crystal structure, DFT calculations, Hirshfeld surface analysis, energy frameworks, molecular dynamics and docking studies of novel isoxazole-quinoxaline derivative (IZQ) as anti-cancer drug, J. Mol. Struct. 1232 (2021) 1–12.

[7] F.H. Al-Ostoot, D.V. Geetha, Y.H.E. Mohammed, P. Akhileshwari, M.A. Sridhar, S.A. Khanum, Design-based synthesis, molecular docking analysis of an anti-inflammatory drug, and geometrical optimization and interaction energy studies of an indole acetamide derivative, J. Mol. Struct. 1202 (2020) 1–11.

[8] T. Prashanth, P. Thirusangu, B.V. Avin, V.L. Ranganatha, B.T. Prabhakar, S.A. Khanum, Synthesis and evaluation of novel benzophenone-thiazole derivatives as potent VEGF-A inhibitors, Eur. J. Med. Chem. 87 (2014) 274–283.

[9] T. Prashanth, B.V. Avin, P. Thirusangu, V.L. Ranganatha, B.T. Prabhakar, J.N.S. Chandra, S.A. Khanum, Synthesis of coumarin analogs appended with quinoline and thiazole moiety and their apoptogenic role against murine ascitic carcinoma, Biomed. Pharmacother. 112 (2019) 1–11.

[10] G. Yang, L. Shi, Z. Pan, L. Wu, L. Fan, C. Wang, C. Xu, J. Liang, The synthesis of coumarin thiazoles containing a trifluoromethyl group and their antifungal activities, Arab. J. Chem. 14 (2021) 1–8.

[11] E. Gürsoy, E.D. Dincel, L. Naesens, N.U. Güzeldemirci, Design and synthesis of novel imidazo [2, 1-b] thiazole derivatives as potent antiviral and antimycobacterial agents, Bioorgan. Chem. 95 (2020) 103496.

[12] S.L. Manju, Identification and development of thiazole leads as COX-2/5-LOX inhibitors through *in-vitro* and *in-vivo* biological evaluation for anti-inflammatory activity, Bioorgan. Chem. 100 (2020) 103882.

[13] Y.H.E. Mohammed, V.H. Malojirao, P. Thirusangu, M. Al-Ghorbani, B.T. Prabhakar, S.A. Khanum, The Novel 4-phenyl-2-phenoxyacetamide thiazoles modulates the tumor hypoxia leading to the crackdown of neoangiogenesis and evoking the cell death, Eur. J. Med. Chem. 143 (2018) 1826–1839.

[14] S.M. Sanad, A.A. Ahmed, A.E. Mekky, Synthesis, *in-vitro* and in-silico study of novel thiazoles as potent antibacterial agents and MurB inhibitors, Arch. Der Pharm. 353 (2020) 1900309.

[15] A. Oluwaseye, A. Uzairu, G.A. Shallangwa, S.E. Abechi, In silico study on anticonvulsant activity of isoxazole and thiazole derivatives active in subcutaneous pentylenetetrazole animal model, J. King Saud. Univ. Sci. 32 (2020) 116–124.

[16] V. Gupta, V. Kant, A review on biological activity of imidazole and thiazole moieties and their derivatives, Sci. Int. 1 (2013) 253–260.

[17] M.V.N. de Souza, Synthesis and biological activity of natural thiazoles: an important class of heterocyclic compounds, J. Sulfur Chem. 26 (2005) 429–449.

[18] A.B. Santos, A.M. Manfredi, C.A. Salla, G. Farias, E. Girotto, J. Eccher, E. Westphal, S.F. Curcio, T. Cazati, I. Malvestiti, E.H. Falcao, Highly luminescent liquid crystals by connecting 1, 3, 4-oxadiazole with thiazolo [5, 4-d] thiazole units, J. Mol. Liq. 321 (2021) 1–10.

[19] M.I. Rogovoy, A.V. Tomilenko, D.G. Samsonenko, N.A. Nedolya, M.I. Rakhmanova, A.V. Artem'ev, New silver (I) thiazole-based coordination polymers: structural and photophysical investigation, Mendeleev Commun. 30 (2020) 728–730.

[20] R. Ujan, A. Bahadur, G. Shabir, S. Iqbal, A. Saeed, P.A. Channar, Q. Mahmood, M. Shoaib, I. Arshad, M. Saifullah, G. Liu, Facile synthesis of novel fluorescent thiazole coumarinyl compounds: electrochemical, time resolve fluorescence, and solvatochromic study, J. Mol. Struct. 1227 (2021) 129422.

[21] Y. Li, Y. Xu, X. Qian, B. Qu, Naphthalimide–thiazoles as novel photonucleases: molecular design, synthesis, and evaluation, Tetrahedron Lett. 45 (2004) 1247–1251.

[22] N.N. Soliman, M. Abd El Salam, A.A. Fadda, M. Abdel-Motaal, Synthesis, characterization, and biochemical impacts of some new bioactive sulfonamide thiazole derivatives as potential insecticidal agents against the cotton leafworm, spodoptera littoralis, J. Agric. Food Chem. 68 (2020) 5790–5805.

[23] H.A. Khamees, Y.H.E. Mohammed, A. Swamynayaka, F.H. Al-Ostoot, Y. Sert, S. Alghamdi, S.A. Khanum, M. Madegowda, Molecular structure, DFT, vibrational spectra with fluorescence effect, Hirshfeld surface, docking simulation and antioxidant activity of thiazole derivative, ChemistrySelect 4 (2019) 4544–4558.

[24] H.A. Khamees, Y.H.E. Mohammed, S. Ananda, F.H. Al-Ostoot, Y. Sangappa, S. Alghamdi, S.A. Khanum, M. Madegowda, Effect of o-difluoro and p-methyl substituents on the structure, optical properties and anti-inflammatory activity of phenoxy thiazole acetamide derivatives: theoretical and experimental studies, J. Mol. Struct. 1199 (2020) 1–18.

[25] G. Sharma, S. Anthal, D.V. Geetha, F.H. Al-Ostoot, Y.H.E. Mohammed, S.A. Khanum, M.A. Sridhar, R. Kant, Synthesis, structure and molecular docking analysis of an anticancer drug of n-(2-aminophenyl)-2-(2-isopropylphenoxy) acetamide, Mol. Cryst. Liq. Cryst. 675 (2018) 85–95.

[26] H.H. Sallam, Y.H.E. Mohammed, F.H. Al-Ostoot, M.A. Sridhar, S.A. Khanum, Synthesis, structure analysis, DFT calculations, Hirshfeld surface studies, and energy frameworks of 6-Chloro-3-[(4-chloro-3-methylphenoxy) methyl][1,2,4] triazolo[4, 3-b]pyridazine, J. Mol. Struct. 1237 (2021) 1–8.

[27] F.H. Al-Ostoot, J. Stondus, S. Anthal, D.V. Geetha, Y.H.E. Mohammed, M.A. Sridhar, S.A. Khanum, R. Kant, Synthesis, spectroscopic and X-ray crystallographic analysis of N-(2-(2-(4-chlorophenoxy) acetamido) phenyl)-1H-indole-2-carboxamide, Eur. J. Chem. 10 (2019) 234–238.

[28] L. Krause, R. Herbst-Irmer, G.M. Sheldrick, D. Stalke, Comparison of silver and molybdenum microfocus X-ray sources for single-crystal structure determination, J. Appl. Crystallogr. 48 (2015) 3–10.

[29] G.M. Sheldrick, Crystal structure refinement with SHELXL, Acta Crystallogr. Sect. C Struct. Chem. 71 (2015) 3–8.

[30] A.L. Spek, Single-crystal structure validation with the program PLATON, J. Appl. Crystallogr. 36 (2003) 7–13.

[31] C.F. Macrae, I.J. Bruno, J.A. Chisholm, P.R. Edgington, P. McCabe, E. Pidcock, L. Rodriguez-Monge, R. Taylor, J.V.D. Streek, P.A. Wood, Mercury CSD 2.0–new features for the visualization and investigation of crystal structures, J. Appl. Crystallogr. 41 (2008) 466–470.

[32] H.H. Sallam, Y.H.I. Mohammed, F.H. Al-Ostoot, M.A. Sridhar, S.A. Khanum, Synthesis, crystal structure characterization, DFT calculations, Hirshfeld surface analysis and 3D energy frameworks of triazole pyridazine derivatives: Theoretical and experimental studies, J. Mol. Struct. 1246 (2021) 1–10.

[33] M.A. Spackman, D. Jayatilaka, Hirshfeld surface analysis, Cryst. Eng. Commun. 11 (2009) 19–32.

[34] D.C. Garwood, D.J. Cram, Properties and maps of stereochemical reaction cycles that involve compounds with four ligands attached to a tetrahedral chiral center, J. Am. Chem. Soc. 92 (1970) 4575–4583.

[35] J.J. McKinnon, D. Jayatilaka, M.A. Spackman, Towards quantitative analysis of intermolecular interactions with Hirshfeld surfaces, Chem. Commun. 37 (2007) 3814–3816.

[36] H.H. Sallam, Y.H.E. Mohammed, D.V. Geetha, F.H. Al-Ostoot, M.A. Sridhar, S.A. Khanum, Synthesis, structural analysis, Hirshfeld surface analysis, DFT calculations, *in vitro* and docking study on antioxidant activity of 6-chloro-3-[(4-methylphenoxy) methyl] [1,2,4] triazolo[4,3-b]pyridazine, Mol. Cryst. Liq. Cryst. (2021) 1–20.

[37] H. Yadav, N. Sinha, B. Kumar, Growth and characterization of piezoelectric benzil single crystals and its application in microstrip patch antenna, CrystEngComm 16 (2014) 10700–10710.

[38] J.J. McKinnon, M.A. Spackman, A.S. Michell, Novel tools for visualizing and exploring intermolecular interactions in molecular crystals, Acta Crystallogr. Section B Struct. Sci. 60 (2004) 627–668.

[39] C.F. Mackenzie, P.R. Spackman, D. Jayatilaka, M.A. Spackman, CrystalExplorer model energies and energy frameworks: extension to metal coordination compounds, organic salts, solvates and open-shell systems, Int. Union Crystallogr. J. 4 (2017) 575–587.

[40] M.J. Turner, S.P. Thomas, M.W. Shi, D. Jayatilaka, M.A. Spackman, Energy frameworks: insights into interaction anisotropy and the mechanical properties of molecular crystals, Chem. Commun. 51 (2015) 3735–3738.